Competing exchange bias and field-induced ferromagnetism in La-doped $BaFeO_3$

I. Fita,[1,*] A. Wisniewski,[1] R. Puzniak,[1] P. Iwanowski,[1] V. Markovich,[2] S. Kolesnik,[3] and B. Dabrowski[3]

[1]*Institute of Physics, Polish Academy of Sciences, Aleja Lotnikow 32/46, PL-02668 Warsaw, Poland*

[2]*Department of Physics, Ben-Gurion University of the Negev, P.O. Box 653, 84105 Beer-Sheva, Israel*

[3]*Department of Physics, Northern Illinois University, DeKalb, Illinois 60115, USA*

(Received 9 January 2017; revised manuscript received 15 March 2017; published 18 April 2017)

An exchange bias (EB) effect was observed in mixed valent $La_xBa_{1-x}FeO_3$ ($x = 0.125, 0.25, 0.33$) perovskites exhibiting the antiferromagnetic (AFM) helical order among Fe^{4+} ions coexisting with the ferromagnetic (FM) cluster phase in the ground state. The La^{3+} ions for Ba^{2+} site substitution, associated with increase in number of the AFM coupled Fe^{3+} - Fe^{4+} pairs as well as some Fe^{3+} - Fe^{3+} pairs, leads to strengthening of the AFM phase and consequently to the alteration of the EB characteristics, which depend on level of the La doping x. At low doping $x \leqslant 0.25$, an abnormal dependence of the EB field, H_{EB}, on the cooling field, H_{cool}, was found. The H_{EB} increases rapidly with increasing cooling field at low H_{cool}, but it falls suddenly at cooling fields higher than 20 kOe, reducing by an order of magnitude at 90 kOe. The suppression of EB is caused by the field-induced increased volume of the FM phase, due to the transformation of the AFM helical spin structure into the FM one. Thus, low-doped $La_xBa_{1-x}FeO_3$ demonstrates a competition of two alternate cooling-field-induced effects, one of which leads to the EB anisotropy and another one to the enhanced ferromagnetism. In contrast, the $x = 0.33$ sample, having a strong AFM constituent, shows no field-induced FM and no drop in the EB field. Accordingly, the H_{EB} vs H_{cool} dependence was found to be well explained in the framework of a model describing phase-separated AFM-FM systems, namely, the model assuming isolated FM clusters of size ~4 nm embedded in the AFM matrix.

DOI: 10.1103/PhysRevB.95.134428

I. INTRODUCTION

$BaFeO_3$ is a representative of an exceptional class of perovskite oxides, $MFeO_3$ (M^{2+} = Ca, Sr, Ba), which contains iron ions in a high valence state of Fe^{4+} ($3d^4$) and shows a tendency toward ferromagnetism (FM) and metallicity, in contrast to nearly all lower Fe valence oxides exhibiting insulating antiferromagnetism (AFM) [1]. While in $CaFeO_3$ and $SrFeO_3$ the FM may be attained under high pressure only, by compressing the lattice volume by about 11% and 5%, respectively [2,3], the genuine FM with a saturated moment of $3.5\mu_B$ per Fe ion was recently found at ambient pressure below 111 K in stoichiometric $BaFeO_3$ with cubic structure [1]. This FM state is accomplished by applying a small magnetic field of ~3 kOe, needed to suppress the original *A*-type helical spin order (comprising both interlayer FM and intralayer AFM orders) in bulk $BaFeO_3$, which is very close in energy to the uniform FM state as observed in thin films [4]. In contrast, a magnetic field higher than 400 kOe is required to achieve the same $3.5\mu_B$ moment in cubic $SrFeO_3$ antiferromagnet with much stronger *G*-type helical order, which demonstrates the existence of several novel competing helimagnetic phases, attractive for applications [5]. The helical spin order may be explained by the double-exchange mechanism which is effective in the case of Fe^{4+} oxides with negative charge transfer energy [6]. It should be noted that the realistic electronic state of the Fe^{4+} ions is rather closer to $d^5\underline{L}$ than d^4, due to the strong *p*-*d* hybridization, giving rise to an itinerant ligand hole $\underline{L}$ in the oxygen *p* orbital [5,7]. It was also reported for $BaFeO_3$ that the magnetic ordering temperature shifts to 300 K under 40 GPa pressure [1], and the electronic structure calculations predicted a robust ferromagnetism far above 300 K [8]. It thus appears that both the effect of lattice expansion (and the related Fe-O bond elongation) due to the increased size of M^{2+} ion and the effect of external pressure, causing the compression of both Ba-O and Fe-O bonds, lead to the ferromagnetism in $MFeO_3$ [1,9]. Recently, complex relationships between *G*-type helical AFM and FM orders have been observed in $SrFeO_3$ by a shift of the magnetization hysteresis loops along the horizontal axis associated with unidirectional exchange anisotropy [10].

In an added complexity, the substitution of M^{2+} ion by higher valence La^{3+} ion drives the system back to the AFM ground state. The AFM ground state develops most probably because of the appearance of AFM interactions between Fe^{4+} and emerging from the electrical neutrality condition the Fe^{3+} ions, as well as because some pairs of Fe^{3+} and Fe^{3+}, known for very strong AFM interactions, are formed [11]. Coexisting FM and AFM phases revealed by a FM cluster-glass behavior below 115 K were observed in cubic $La_{0.5}Ba_{0.5}FeO_3$ [12]. It is interesting to investigate similar exchange interaction effects on the interface between FM and AFM phases, comprising a helical spin structure in other mixed valent perovskites with varying Fe^{3+}/Fe^{4+} ratios.

In this paper, we report on a strong exchange bias (EB) effect in a La-substituted for Ba system $La_xBa_{1-x}FeO_3$ ($x = 0.125 - 0.33$), which is intermediate between $BaFeO_3$ and $La_{0.5}Ba_{0.5}FeO_3$. For low-doped samples $x \leqslant 0.25$, the EB field, H_{EB}, was found to increase in absolute value rapidly at small cooling field, H_{cool}, but it falls abruptly at higher H_{cool} due to the field-induced ferromagnetism. In contrast, the $x = 0.33$ sample with a strong AFM constituent shows no field-induced FM and the H_{EB} vs H_{cool} dependence which is

*Corresponding author: ifita@ifpan.edu.pl

reminiscent of that commonly observed for system of isolated FM clusters embedded in an AFM matrix.

II. SAMPLE PREPARATION AND EXPERIMENTAL PROCEDURES

Polycrystalline samples of $La_xBa_{1-x}FeO_{3-d}$ ($x = 0.125$, 0.25, 0.33) have been obtained by a solid-state synthesis method from stoichiometric mixtures (all 99.999%) of Fe_2O_3, $BaCO_3$, and La_2O_3 dried in air. Samples were pressed into pallets and fired in air at increasing temperatures from 1000 °C to 1300 °C with several intermediate regrindings. The final firings were done at 1300 °C followed by quenching in liquid nitrogen to obtain a single-phase oxygen-deficient perovskite phase with $d > 0$. These oxygen-deficient samples were subsequently annealed in air at 350 °C, at high oxygen pressure of 160 atm at 400 °C, and finally at 500 atm at 450 °C, followed by very slow cooling to room temperature, at a rate of 6 deg/h. The oxygen content in the samples was determined from the mass change between various annealings. The structure was monitored by x-ray diffraction using a Rigaku D/MAX powder diffractometer after each synthesis step. The $x = 0.125$, 0.25, and 0.33 samples were found to be single-phase cubic Pm-$3m$ with lattice parameters $a = 3.974$, 3.950, and 3.947 Å, respectfully. Room temperature x-ray diffraction patterns of cubic $La_xBa_{1-x}FeO_3$ are presented in Fig. 1.

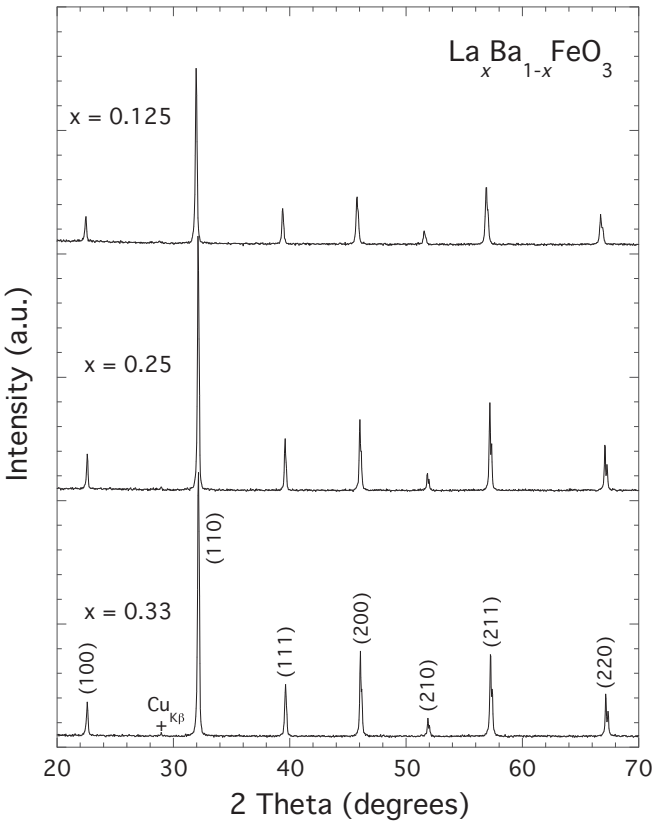

FIG. 1. Room temperature x-ray diffraction patterns of cubic $La_xBa_{1-x}FeO_3$. The diffraction peak near 29 deg (denoted by cross) results from incompletely screened copper K_β radiation of the (110) peak.

Obtaining fully oxygenated $La_xBa_{1-x}FeO_3$ samples is difficult for $x < 0.5$. Repeated annealings in air are necessary for $x = 0.5$ (Ref. [12]), whereas electrochemical oxidation or annealing in ozone is required for $BaFeO_3$ ($x = 0$) (Ref. [1]). Both these compounds are cubic with $a = 3.93$ and ~3.97 Å, respectively. Our final annealing in oxygen at 500 atm and 450 °C should result in the fully stoichiometric materials studied here. We note, however, that we were not able to achieve a cubic $BaFeO_3$ sample, indicating that annealing in oxygen at 500 atm is not sufficient to obtain a stoichiometric $x = 0$ sample.

The increase of the lattice parameter a with the heterovalent substitution of Ba^{2+} for La^{3+} is unusual for perovskites. Increasing Ba substitution in $La_xBa_{1-x}FeO_3$ is compensated by decreasing population of e_g electrons on the Fe site, resulting in a decreasing ionic size of Fe. Typically, such substitutions lead to a decrease of lattice parameters for the ABO_3 perovskites. However, since all compositions $x = 0 - 0.5$ are cubic, the substitution of larger Ba for smaller La is accommodated by elongation of the Fe-O bonds and the increase of lattice parameter a, irrespective of the particular valence and size of Fe. The resulting materials thus contain Fe-O bonds elongated beyond equilibrium values, which is a consequence of the two-step, reduction–oxidation synthesis method. Similar methods were used, for example, to obtain multiferroic manganites with elongated Mn-O bonds [13].

Magnetization measurements, such as temperature dependences and hysteresis loops in both field-cooling (FC) and zero-field-cooling (ZFC) modes, were performed in the temperature range $10 - 300$ K in the magnetic field up to 90 kOe using the VSM option of the Physical Property Measurement System (PPMS) of Quantum Design.

III. RESULTS AND DISCUSSION

Figure 2(a) presents the temperature dependences of both ZFC and FC magnetization for $La_xBa_{1-x}FeO_3$ measured at

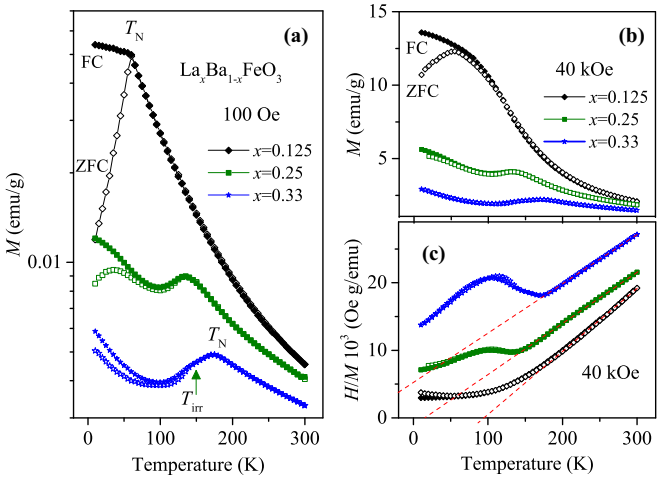

FIG. 2. Temperature dependences of ZFC (open symbols) and FC (solid symbols) magnetization for $La_xBa_{1-x}FeO_3$ measured (a) at 100 Oe, presented in log scale, and (b) at 40 kOe. (c) Inverse susceptibility H/M measured at 40 kOe. The Curie-Weiss fit is shown by a dashed line.

100 Oe. These M vs T curves demonstrate an evolution of the AFM state with increasing La content x in the system. Magnetic transition temperature, T_N, increases from 60 K for $x = 0.125$ to 135 K for $x = 0.25$, and to 175 K for $x = 0.33$, while the FC magnetization at 10 K decreases by an order of magnitude. A strong gap between ZFC and FC magnetization branches just below T_N in the $x = 0.125$ sample may be assigned to the inhomogeneous magnetic state due to the coexisting AFM and FM orders, leading to a glassy-like magnetic behavior. For larger La doping, this inhomogeneous AFM/FM state, indicated by irreversibility in ZFC and FC curves, occurs at temperature T_{irr}, which is distinctly lower than the Néel temperature T_N defined by a maximum in M [see example of $x = 0.33$ in Fig. 2(a)]. The ZFC-FC divergence exists as well at a high magnetic field of 40 kOe in low-doped samples, presented in Fig. 2(b), and even at fields up to 90 kOe, due to the cooling-field-induced FM phase in a helical AFM spin structure, as will be shown later. The inverse susceptibility H/M follows the Curie-Weiss law $M/H = C/(T - \theta)$ in a paramagnetic temperature range, between 200 and 300 K, shown in Fig. 2(c) together with the fit to the data. The parameters obtained from the fit are $C = 2.58$, 3.19, 3.25 (emu K/mol Oe) and $\theta = 94$, 14, -65 K for $x = 0.125$, 0.25, 0.33, respectively. The change of sign in Curie-Weiss temperature θ indicates that AFM interactions become dominant in $La_xBa_{1-x}FeO_3$ at $x = 0.33$, which is consistent with the increase in the Néel temperature T_N with increasing La doping. For comparison, the positive Curie-Weiss temperature $\theta = 163$ K, consistent with our data, has been derived for pure $BaFeO_3$ [14]. The doping effect may be explained by the increased number of the AFM Fe^{3+} - Fe^{4+} and Fe^{3+} - Fe^{3+} pairs in the system [11]. An increased contribution from the Fe^{3+} species with larger spin $S = 5/2$, as compared with that for Fe^{4+}, $S = 2$, is evidenced by the increase in the effective magnetic moment μ_{eff} per Fe ion from $4.54\mu_B$ for $x = 0.125$ to $5.1\mu_B$ for $x = 0.33$, where μ_{eff} is calculated by applying the equation $C = N_A\mu_{eff}^2/3k_B$, where N_A and k_B are Avogadro and Boltzmann constants, respectively.

Magnetization hysteresis loops of $La_xBa_{1-x}FeO_3$ for $x = 0.125$, 0.25, and 0.33 at 10 K measured with several cooling fields H_{cool} are presented in Figs. 3(a), 4(a), and 4(b). Two important features are revealed from the hysteresis loops: (i) even at small H_{cool}, the FC loop changes its shape and shifts away from the origin, due to the exchange bias anisotropy; (ii) at H_{cool} higher than 20 kOe, the high-field magnetization starts to increase due to the cooling-field-induced ferromagnetism, leading to a progressive suppression of the exchange bias effect with increasing H_{cool}.

The ZFC hysteresis loops of the samples with different FM-to-AFM phase ratio are strictly symmetric, showing a small coercive field, H_C, while the magnetization at the highest field applied at 10 K is far from the expected for saturated moment of $3.5\mu_B$. Even for $x = 0.125$ sample, with the highest FM contribution, M reaches value of $0.8\mu_B$ at 90 kOe; therefore, the full saturation is expected at much higher fields. For comparison, for the G-type helical AFM $SrFeO_3$ with moment of $\sim 0.4\mu_B$ at 90 kOe, the saturated moment of $3.5\mu_B$ is achieved at 4 K only with an applied pulse magnetic field of about 400 kOe [5].

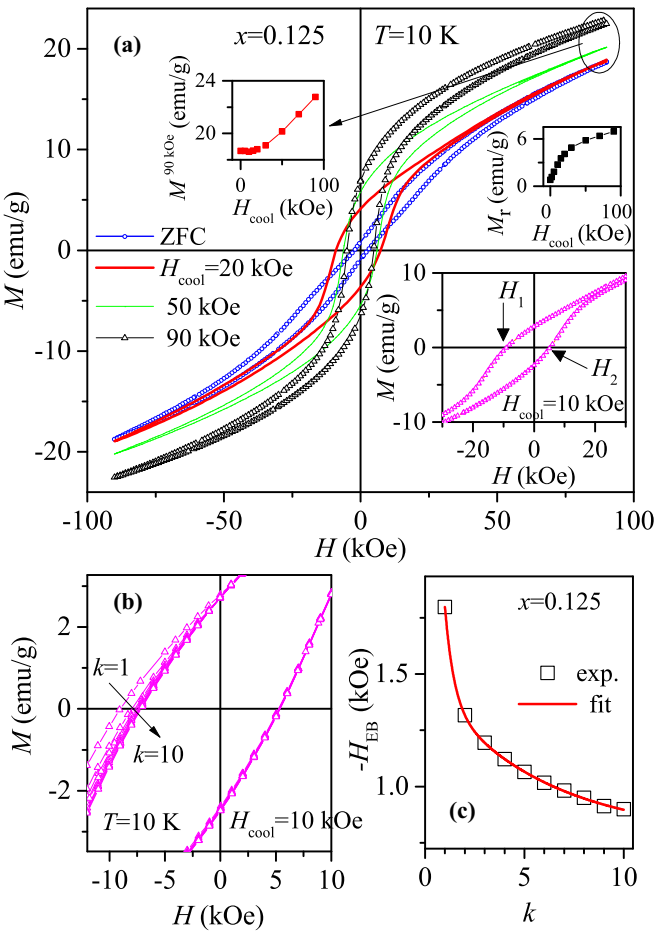

FIG. 3. (a) Magnetization hysteresis loops of $La_{0.125}Ba_{0.875}FeO_3$ at 10 K measured with several cooling fields H_{cool}. The upper insets show the cooling-field-induced increase in (left) magnetization at 90 kOe and (right) remanent magnetization at $H = 0$, and the lower inset presents an FC loop with $H_{cool} = 10$ kOe over an extended scale. (b) Detailed picture of ten loop measurements performed consecutively between ±90 kOe at 10 K after cooling in a field of 10 kOe. (c) Field H_{EB} (see text) at 10 K versus increasing number of recurrent hysteresis loops k; the solid line represents the best fit with Eq. (1).

It is seen in Figs. 3 and 4 that much stronger changes in field-dependent magnetization occur when following the field-cooling process as compared to that obtained after ZFC. One reason for such behavior is the EB anisotropy emerging at the interface between interacting FM and AFM phases [15]. The EB effect is evidenced in a shift of the hysteresis loop away from the origin, which happens after FC [see insets in Figs. 3 and 4]. The hysteresis loops also widen under FC, indicating the increase in both coercive field and remanent magnetization. The EB field, defined as $H_{EB} = (H_1 + H_2)/2$, is negative, as typically occurs for applied positive H_{cool} [16], while the average coercive field $H_C = (H_2 - H_1)/2$ presents a half of the loop width, where H_1 and H_2 are the negative and positive coercive fields at the first and second magnetization reversals, respectively. At 10 K and at relatively small $H_{cool} = 10$ kOe, the $|H_{EB}|$ achieves values of 1.89, 1.45, and 0.46 kOe for $x = 0.125$, 0.25, and 0.33 samples,

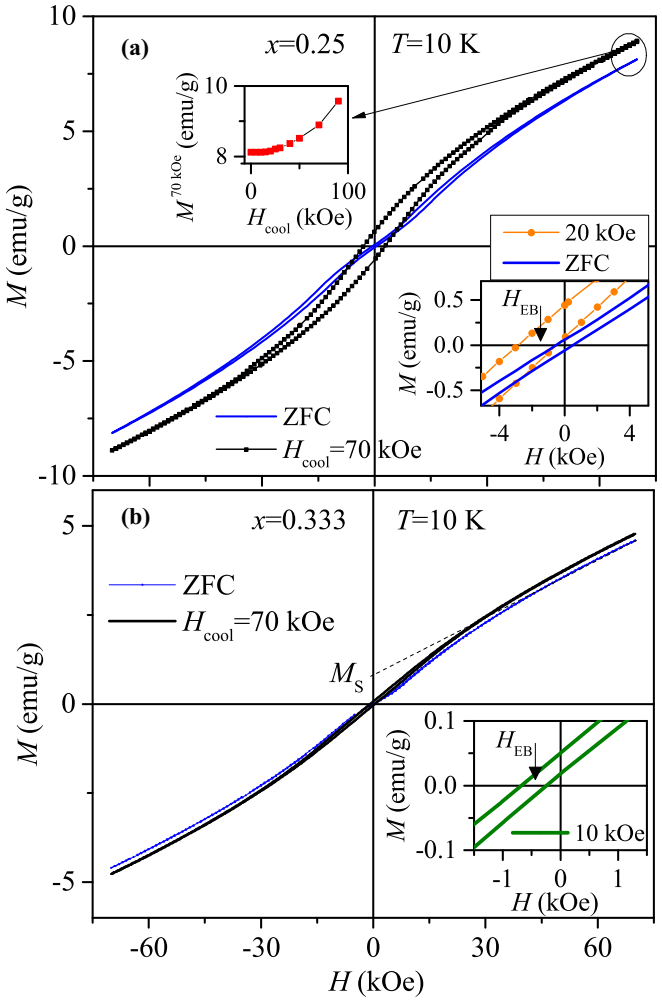

FIG. 4. (a) Magnetization hysteresis loops for $La_{0.25}Ba_{0.75}FeO_3$ at 10 K measured with ZFC mode and with $H_{cool} = 70$ kOe. Upper inset shows the cooling-field-induced increase in magnetization at 70 kOe, and the lower inset presents both symmetric ZFC and shifted FC ($H_{cool} = 20$ kOe) loops in an extended scale. (b) ZFC and FC ($H_{cool} = 70$ kOe) loops for $La_{0.33}Ba_{0.67}FeO_3$ at 10 K. Inset shows a shift of the $H_{cool} = 10$ kOe loop in an extended scale.

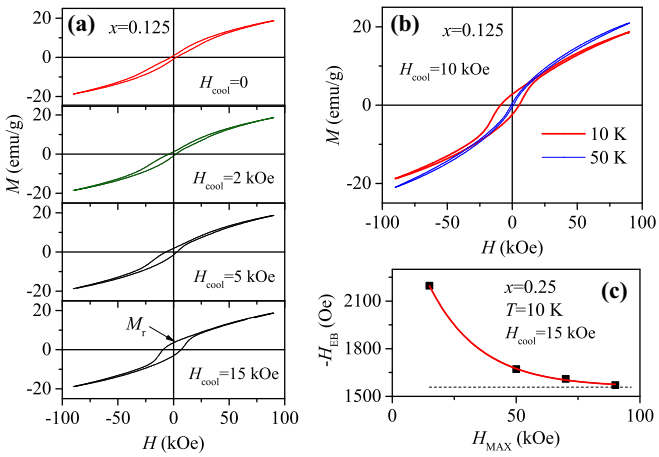

FIG. 5. (a) Evolution of hysteresis loop of $La_{0.125}Ba_{0.875}FeO_3$ at 10 K with increasing cooling field H_{cool}. (b) Hysteresis loops of $La_{0.125}Ba_{0.875}FeO_3$ measured with $H_{cool} = 10$ kOe at 10 and 50 K. (c) H_{EB} field as a function of the maximum field of the loop H_{MAX} measured with constant $H_{cool} = 15$ kOe for $La_{0.25}Ba_{0.75}FeO_3$ at 10 K. Solid line represents exponential fit, and the dashed line indicates the asymptotic value $H_{EB}(H_{MAX} \to \infty)$ which is intrinsic H_{EB}.

respectively. With increasing temperature, the $|H_{EB}|$ decreases monotonically and becomes zero at temperature T_{irr}, below which both AFM and FM phases coexist.

It is noteworthy that even a small cooling field strongly affects the magnetic state, as evidenced in Fig. 5(a) by evolution of the hysteresis loop with increasing H_{cool}. The ZFC loop shows a clear dual-loop behavior, namely, the loop is composed of two subloops, one shifted to positive fields and the other to negative ones. This effect is usually observed when the exchange-biased FM/AFM system is zero-field cooled in a demagnetized state [17,18]. In this case, the FM domains of opposite magnetization direction may be frozen, leading to the existence in the sample of two equal-in-value EB fields of opposite sign, each of which provides the shift of the loop in opposite directions—this mechanism is responsible for the formation of a dual loop [17]. Under FC, the FM moments directed oppositely to the applied field are suppressed while the number of moments along the field increases; therefore, with increasing H_{cool}, the subloop originating from the positive EB progressively collapses and the subloop with negative EB grows and transforms into the single loop with large values of H_C and remanent magnetization M_r [see evolution of the loop in Fig. 5(a)]. Thus, for $La_xBa_{1-x}FeO_3$, the hysteresis loop shape may be varied from a dual loop to the single one by varying the cooling field.

Another field-induced effect, which is triggered by higher cooling fields, is seen from the hysteresis loops for the $x = 0.125$ sample, as presented in Fig. 3(a). The magnetization at field of 90 kOe, applied at 10 K, almost coincides for all loops with cooling fields between zero and 20 kOe, but it starts to increase for loops with H_{cool} larger than 20 kOe [see left inset in Fig. 3(a)]. It appears that the application of a cooling field of 90 kOe enhances the magnetization by ~25% in comparison to that obtained by the same field applied at 10 K. A very similar behavior, though with smaller effect (~18%), was observed for $x = 0.25$ doping, while a negligible effect was found for $x = 0.33$ composition with the strongest AFM component [see Fig. 4(a) and inset in Fig. 4(a)]. We suggest that the field-induced increase of magnetization in $La_xBa_{1-x}FeO_3$ is due to the partial transformation of the AFM screw spin structure into the FM one, similar to that occurring in a $SrFeO_3$ helical magnet [5]. In the case of $SrFeO_3$, this field-induced ferromagnetism develops continuously through an intermediate spin structure in interval of fields between 200 and 400 kOe at 4 K. At temperature of 120 K, which is close to the transition into paramagnetic phase, the ferromagnetism develops at lower fields between 80 and 120 kOe. Thus, it seems that the FM phase expands progressively when the magnetic field is applied at higher temperatures. Additional magnetization emerging during the FC process for low-doped $La_xBa_{1-x}FeO_3$ can be possibly explained by similar behavior. Other evidences for the cooling-field-induced ferromagnetism are both strong change of the loop shape from nearly AFM type (dual loop) to the clear FM type and an increase in the remanent

magnetization M_r by an order of magnitude [see right upper inset in Fig. 3(a)], with increasing H_{cool} from zero to 90 kOe. It appears that the extra FM phase emerges in the sample, as a result of the FC process, and then it persists at $T = 10$ K during the magnetization circle. It also should be noted that the cooling-field-induced magnetization appears to be larger when the field of 90 kOe is applied at higher temperature below T_N [see Fig. 5(b)].

It should be stressed that a proper estimation of the EB parameters in strongly anisotropic systems is problematic when the magnetization remains unsaturated, even at high magnetic field, and in this case the minor hysteresis loops may exhibit shift which has nothing in common with the real EB [16]. However, it was suggested that the existence of "true" EB in similar systems may be verified by "effectively saturated" hysteresis loops [19,20]. A system is considered to be effectively saturated when the ascending and descending branches of the loop coincide at fields higher than the anisotropy field. The appropriate value of the maximum field of the loop H_{MAX}, at which the minor loop effect is sufficiently small, can be estimated by measuring the H_{EB} field as a function of H_{MAX} at constant parameters T and H_{cool}. The H_{EB} vs H_{MAX} dependence for the $x = 0.25$ sample is presented in Fig. 5(c). The solid line represents an exponential fit and the dashed line indicates the asymptotic value $H_{EB}(H_{MAX} \rightarrow \infty) = 1560$ Oe, which is intrinsic H_{EB}. This procedure shows that the H_{EB} measured with $H_{MAX} = 90$ kOe differs by ~1% only from the true value of H_{EB}.

The EB behavior was verified by measurements of the training effect, which is revealed usually by the reduction of H_{EB}, due to the AFM domain rearrangement at the interface, with repetition of the hysteresis loop at a fixed temperature [16,21,22]. Figure 3(b) presents a narrow range of ten hysteresis loops performed consecutively for the $x = 0.125$ composition between ±90 kOe at 10 K after cooling in the field $H_{cool} = 10$ kOe. The field H_{EB} was found to diminish by a factor of 2 with training by ten repeated magnetization cycles, as shown in Fig. 3(c). The relaxation of the H_{EB} as a function of the number of cycles k may be simulated within the framework of the spin-configuration relaxation model [23], in which two different types of AFM uncompensated spins, the first one frozen and the second one rotatable, are exchange-coupled to the AFM and FM layers, respectively:

$$H_{EB}(k) = H_{EB}(k \rightarrow \infty) + A_f \exp(-k/P_f) + A_i \exp(-k/P_i), \quad (1)$$

where A_f and P_f are parameters related to the changes in the frozen spins, and A_i and P_i are evolving parameters linked to the rotatable spin component at the FM/AFM interface (here, parameter P is indicative of the relaxation rate). The solid line in Fig. 3(c) is the best fit of Eq. (1) to the $H_{EB}(k)$ data with fitting parameters $H_{EB}(k \rightarrow \infty) = -0.78$ kOe, $A_f = -0.70$ kOe, $P_f = 5.6$, $A_i = -3.9$ kOe, and $P_i = 0.46$. It shows that a contribution from the rotatable uncompensated AFM spins at the interface is predominant at the initial stage of training, while the frozen AFM component is much weaker and relaxes about 10 times slower as compared to the rotatable one.

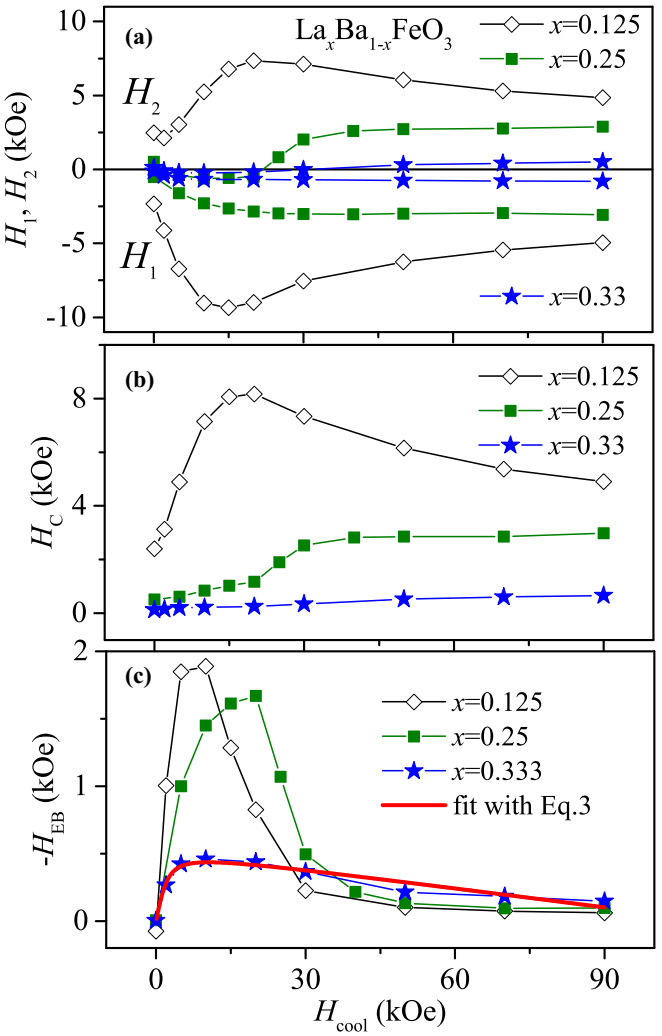

FIG. 6. (a) Variation of the coercive fields H_1 and H_2 with cooling field H_{cool} in $La_xBa_{1-x}FeO_3$ at 10 K. (b) The average coercive field H_C versus H_{cool}. (c) Cooling-field dependence of exchange bias field H_{EB} at 10 K. Bold line represents the best fit with use of Eq. (3), calculated for a system of FM clusters (size of 4.2 nm) embedded in an AFM matrix.

Further insight into evolution of the EB in $La_xBa_{1-x}FeO_3$ samples is obtained from the dependence of hysteresis loops on the cooling field H_{cool}. Figure 6(a) presents the variation dependence of the coercive fields H_1 and H_2 on H_{cool}, while the variation of the average coercive field H_C is shown in Fig. 6(b). Remarkably, the field of the second magnetization reversal, H_2, exhibits a minimum at low H_{cool}; moreover, the H_2 becomes negative in the $x = 0.25$ and $x = 0.33$ samples at cooling fields smaller than 20 and 30 kOe, respectively. This behavior signifies that the cooling-field-induced EB anisotropy dominates at relatively small H_{cool}. Figure 6(c) shows that the absolute value of EB field $|H_{EB}|$ increases rapidly with increasing H_{cool}, as it does generally for the exchange-biased systems, but suddenly $|H_{EB}|$ falls sharply in the $x = 0.125$ and $x = 0.25$ samples, when H_{cool} becomes larger than 10 and 20 kOe, respectively. In contrast, the $x = 0.33$ sample shows no drop in $|H_{EB}|$, and its $H_{EB}(H_{cool})$ dependence is very similar to that often observed in phase-separated EB systems [24].

We suggest that the suppression of EB at higher H_{cool} values for low-doped $La_xBa_{1-x}FeO_3$ is due to the proposed above cooling-field-induced ferromagnetism. Indeed, by comparing Fig. 6(c) and the left upper insets of Figs. 3(a) and 4(a), one can see that for the samples with $x = 0.125$ and $x = 0.25$, the $|H_{EB}|$ collapses with increasing H_{cool}, at the same H_{cool} values at which the additional magnetization starts to increase distinctly. In addition, no field-induced FM and no drop in $|H_{EB}|$ occur for the $x = 0.33$ sample, consistent with previous discussion. Therefore, there is a competition of two different cooling-field-induced effects, leading to the EB anisotropy and extra ferromagnetism, in low-doped $La_xBa_{1-x}FeO_3$. It should be noted that a competition between EB and ferromagnetism is quite natural for the classic EB effect associated with interfacial exchange interaction between strongly anisotropic AFM and soft FM phases, and it can be well understood within the simple Meiklejohn-Bean model [15]. Within this model the H_{EB} is determined by the ratio of the interfacial exchange energy J to the product of magnetization M_{FM} and the thickness t_{FM} of the FM layers, and depends on both AFM anisotropy, K_{AFM}, and thickness of the AFM layers, t_{AFM}, as follows [21]:

$$H_{EB} = \begin{cases} (-J/M_{FM}t_{FM})(1 - 1/4R^2)^{1/2} & \text{for } R \geqslant 1 \\ 0 & \text{for } R < 1, \end{cases} \quad (2)$$

where the parameter $R \equiv K_{AFM}t_{AFM}/J$ determines the region of existing EB in the system, namely, the EB exists only when $R \geqslant 1$, i.e., when the AFM anisotropy energy $K_{AFM}t_{AFM}$ is large enough. In other words, the AFM phase must be strong enough to be able to pin the soft FM phase, thus leading to the EB effect. Regarding our phase-separated system as a system of isolated FM clusters of size D embedded in the AFM matrix, one needs to replace the thickness t_{FM} by $D/6$ and the thickness t_{AFM} by the distance between FM clusters [16]. Within this model, the dramatic changes in EB in low-doped $La_xBa_{1-x}FeO_3$ may be qualitatively explained by significant changes in the FM-to-AFM phase ratio, produced by the cooling field increase from 20 to 90 kOe. The cooling-field-induced expansion of FM phase (~25% and ~18% for $x = 0.125$ and $x = 0.25$, respectively) results in a substantial increase of the FM cluster size D and, simultaneously, it leads to shortening the distance between FM clusters, so that the AFM anisotropy energy $K_{AFM}t_{AFM}$ weakens. It may be suggested that there is a critical distance between FM clusters, analogous to the critical AFM thickness $t^{cr}_{AFM} = J/K_{AFM}$ below which the EB cannot exist, in accordance with Eq. (2). The critical thickness t^{cr}_{AFM} was confirmed experimentally to be inversely proportional to the AFM anisotropy and was found to be about 20 Å only in the case of strongly anisotropic FeF_2/Fe bilayers [25]. Such a small distance between FM clusters is not realistic in $La_xBa_{1-x}FeO_3$ because the magnetic moment even at field of 90 kOe is far from saturation. Therefore, shortening the distance between FM clusters does not significantly affect the EB, and we suppose that the major factor responsible for EB suppression is the cooling-field-induced expansion of the FM cluster size.

Completely different $H_{EB}(H_{cool})$ dependence is observed for the composition with the highest doping $x = 0.33$. This sample shows the highest Néel temperature $T_N = 175$ K, the strongest AFM interactions (θ = -65 K), and the smallest FM phase fraction $M_S = 0.78$ emu/g $= 0.0337\mu_B$/f.u. at $T = 10$ K (as obtained by interpolation of the high-field linear part of M on H dependence to $H = 0$ [see Fig. 4(b)]). It is expected that the helical AFM spin structure at this doping is the hardest as compared to that in low-doped samples; therefore the field-induced transformation from the AFM to FM state does not occur within cooling fields up to 90 kOe. Consequently, the FM-to-AFM phase ratio does not change noticeably, and no drop in $|H_{EB}|$ occurs for $x = 0.33$. Below the temperature of phase separation $T_{irr} = 150$ K [see Fig. 2(a)], the magnetic system at this doping may be regarded as a system of small FM clusters distributed inside the dominant AFM phase. Considering the $H_{EB}(H_{cool})$ dependence, an estimation of the average size of the FM clusters may be obtained within the model proposed in (Ref. [26]) for phase-separated systems consisting of single-domain FM clusters embedded in the AFM matrix:

$$H_{EB} \propto J[(J\mu_0/(g\mu_B)^2)L(\mu H_{cool}/k_B T_f) + H_{cool}], \quad (3)$$

where J is the interface exchange constant, $g \approx 2$ is the gyromagnetic factor, μ_B is the Bohr magneton, L denotes the Langevin function, $\mu_0 \approx 3.5\mu_B$ is the magnetic moment per Fe ion spin, $\mu = N\mu_0$ is the magnetic moment of the FM clusters with N number of spins within the cluster, and $T_f \approx 150$ K is the temperature below which both FM and AFM interacting phases coexist and the EB appears. Equation (3) has been successfully used for evaluation of the FM cluster size in a variety of exchange-biased phase-separated systems, such as manganites and cobaltites [24]. The solid line in Fig. 6(c) represents the best fit with Eq. (3) obtained for the values of fitting parameters $N = 640 \pm 150$ and $J \approx$ -10 $\pm$ 2 K for the $x = 0.33$ sample. By assuming calculated value of N, the FM cluster size of $D \approx 4.2$ nm has been derived. The exchange interaction across the interface J appears to be of the AFM nature. The negative sign of J is responsible for the decrease in $|H_{EB}|$ at high field, according to Eq. (3). One can estimate the density of FM clusters n by considering the spontaneous magnetization $M_S = nN\mu_0$. Taking $M_S = 0.78$ emu/g $= 0.0337\mu_B$/f.u. found at 10 K [see Fig. 4(b)], we estimate the density of FM clusters in $La_{0.33}Ba_{0.67}FeO_3$ to be $n \approx 1.5\times10^{-5}$ f.u.$^{-1}$.

Let us discuss briefly the cooling-field effect on $La_xBa_{1-x}FeO_3$ magnetism, which has a twofold consequence involving both the field-induced ferromagnetism and the EB anisotropy. With increasing cooling field, the EB increases at small H_{cool} but it is suppressed at high H_{cool} due to expansion of the FM phase volume caused by the partial transformation of the AFM helical spin structure into the FM one. Such EB suppression is understandable in view that the applied magnetic field of high enough value must ultimately destroy the AFM structure and, consequently, the EB. For instance, the complete suppression of the EB effect due to the magnetic-field-induced metamagneticlike transition was observed in $CaMn_{0.9}Nb_{0.1}O_3$ manganite [27]. Like in the case of $La_xBa_{1-x}FeO_3$, a fast increase in EB field $|H_{EB}|$ at small H_{cool} and gradual diminution of $|H_{EB}|$ at higher cooling fields have been observed in a granular system of Fe nanoparticles, in which the EB originates from the interfacial interaction between the FM and spin-glass (SG) phases [28]. The authors explained that the strong cooling field, tending

to orient spins along the field direction, strongly modifies the spin configuration of the SG phase, so the Zeeman energy may overcome the interfacial exchange coupling leading to the EB suppression [28]. An extreme cooling-field effect on EB has been observed in FeF_2-Fe bilayers [29]. It was found that the EB is negative at small cooling fields, but it becomes positive for large H_{cool}. The behavior was explained considering that the FeF_2 surface spins couple to the cooling field above T_N and the FeF_2-Fe interaction is AFM [29].

IV. CONCLUSIONS

In summary, the exchange bias effect has been investigated in helical magnets $La_xBa_{1-x}FeO_3$ ($x = 0.125$, 0.25, 0.33) exhibiting the FM-AFM phase-separated ground state with phase ratio varying with doping x. With increasing x, the AFM component, comprised of helical spin order, becomes stronger due to the increase in number of the AFM coupled Fe^{3+} - Fe^{4+} and Fe^{3+} - Fe^{3+} pairs. At low doping $x \leqslant 0.25$, an abnormal dependence of the EB field, H_{EB}, on cooling field, H_{cool}, was found. The H_{EB} increases rapidly at low H_{cool}, but it falls suddenly at cooling fields higher than 20 kOe, decreasing by an order of magnitude at 90 kOe. The suppression of EB is caused by the field-induced increase in the FM phase volume fraction due to the partial transformation of the AFM helical spin structure into the FM one. The low-doped $La_xBa_{1-x}FeO_3$ demonstrates a competition of two dissimilar cooling-field-induced effects, one of which leads to the EB anisotropy and another, effective at higher cooling fields, bringing the enhanced ferromagnetism in the compound. In contrast, the $x = 0.33$ sample with strong AFM constituent shows no field-induced ferromagnetism and no drop in EB within cooling fields up to 90 kOe. Consequently, the H_{EB} vs H_{cool} dependence is well described by the standard model for a system consisting of isolated FM clusters of size ∼4 nm embedded in the AFM matrix.

ACKNOWLEDGMENT

This work was partially supported by the Polish NCN through Grant No. 2014/15/B/ST3/03898, by the EAgLE international project (FP7-REGPOT-2013-1, Project No. 316014) and the international project co-financed by Polish Ministry of Science and Higher Education, Grant Agreement 2819/7.PR/2013/2.

[1] N. Hayashi, T. Yamamoto, H. Kageyama, M. Nishi, Y. Watanabe, T. Kawakami, Y. Matsushita, A. Fujimori, and M. Takano, Angew. Chem. Int. Ed. **50**, 12547 (2011).
[2] T. Kawakami and S. Nasu, J. Phys.: Condens. Matter **17**, S789 (2005).
[3] T. Kawakami, S. Nasu, T. Sasaki, K. Kuzushita, S. Morimoto, S. Endo, T. Yamada, S. Kawasaki, and M. Takano, Phys. Rev. Lett. **88**, 037602 (2002).
[4] S. Chakraverty, T. Matsuda, N. Ogawa, H. Wadati, E. Ikenaga, M. Kawasaki, Y. Tokura, and H. Hwang, Appl. Phys. Lett. **103**, 142416 (2013).
[5] S. Ishiwata, M. Tokunaga, Y. Kaneko, D. Okuyama, Y. Tokunaga, S. Wakimoto, K. Kakurai, T. Arima, Y. Taguchi, and Y. Tokura, Phys. Rev. B **84**, 054427 (2011).
[6] M. Mostovoy, Phys. Rev. Lett. **94**, 137205 (2005).
[7] M. Abbate, G. Zampieri, J. Okamoto, A. Fujimori, S. Kawasaki, and M. Takano, Phys. Rev. B **65**, 165120 (2002).
[8] I. V. Maznichenko, S. Ostanin, L. V. Bekenov, V. N. Antonov, I. Mertig, and A. Ernst, Phys. Rev. B **93**, 024411 (2016).
[9] Z. Li, R. Laskowski, T. Iitaka, and T. Tohyama, Phys. Rev. B **85**, 134419 (2012).
[10] S. Srinath, M. M. Kumar, M. L. Post, and H. Srikanth, Phys. Rev. B **72**, 054425 (2005).
[11] S. Mori, J. Phys. Soc. Jpn. **28**, 44 (1970).
[12] S. Zhang, S. Tan, L. Pi, and Y. Zhang, J. Magn. Magn. Mater. **322**, 3381 (2010).
[13] B. Dabrowski, O. Chmaissem, M. Mais, S. Kolesnik, J. D. Jorgensen, and S. Short, J. Solid State Chem. **170**, 154 (2003); D. K. Pratt, J. W. Lynn, J. Mais, O. Chmaissem, D. E. Brown, S. Kolesnik, and B. Dabrowski, Phys. Rev. B **90**, 140401(R) (2014).
[14] M. Mizumaki, K. Yoshii, N. Hayashi, T. Saito, Y. Shimakawa, and M. Takano, J. Appl. Phys. **114**, 073901 (2013).
[15] W. H. Meiklejohn and C. P. Bean, Phys. Rev. **102**, 1413 (1956); **105**, 904 (1957); W. H. Meiklejohn, J. Appl. Phys. **33**, 1328 (1962).
[16] J. Nogués, J. Sort, V. Langlais, V. Skumryev, S. Suriñach, J. S. Muñoz, and M. D. Baró, Phys. Rep. **422**, 65 (2005).
[17] P. Miltényi, M. Gierlings, M. Bamming, U. May, G. Güntherodt, J. Nogués, C. Leighton, and I. K. Schuller, Appl. Phys. Lett. **75**, 2304 (1999).
[18] S. Brück, J. Sort, V. Baltz, S. Suriñach, J. S. Muñoz, B. Dieny, M. D. Baró, and J. Nogués, Adv. Mater. **17**, 2978 (2005).
[19] J. Geshev, J. Appl. Phys. **105**, 066108 (2009).
[20] J. Geshev, J. Phys.: Condens. Matter **21**, 078001 (2009).
[21] F. Radu and H. Zabel, in *Magnetic Heterostructures: Advances and Perspectives in Spin Structures and Spin Transport*, edited by H. Zabel and S. D. Bader, Springer Tracts in Modern Physics Vol. 227 (Springer-Verlag, Berlin, 2008), pp. 97–184.
[22] A. Hoffmann, Phys. Rev. Lett. **93**, 097203 (2004).
[23] S. K. Mishra, F. Radu, H. A. Dürr, and W. Eberhardt, Phys. Rev. Lett. **102**, 177208 (2009).
[24] S. Giri, M. Patra, and S. Majumdar, J. Phys.: Condens. Matter **23**, 073201 (2011).
[25] M. S. Lund, W. A. A. Macedo, Kai Liu, J. Nogués, I. K. Schuller, and C. Leighton, Phys. Rev. B **66**, 054422 (2002).
[26] D. Niebieskikwiat and M. B. Salamon, Phys. Rev. B **72**, 174422 (2005).
[27] V. Markovich, I. Fita, A. Wisniewski, R. Puzniak, P. Iwanowski, C. Martin, G. Jung, and G. Gorodetsky, Mater Chem. Phys. **164**, 170 (2015).
[28] L. Del Bianco, D. Fiorani, A. M. Testa, E. Bonetti, and L. Signorini, Phys. Rev. B **70**, 052401 (2004).
[29] J. Nogués, D. Lederman, T. J. Moran, and I. K. Schuller, Phys. Rev. Lett. **76**, 4624 (1996).